Dalton Transactions

ROYAL SOCIETY OF CHEMISTRY

PAPER

View Article Online
View Journal | View Issue

Check for updates

Cite this: *Dalton Trans.*, 2022, **51**, 17664

Bulky ligands protect molecular ruby from oxygen quenching†

Laura Stein,[a] Cui Wang,[b] Christoph Förster,[a] Ute Resch-Genger[b] and Katja Heinze*[a]

Received 8th September 2022,
Accepted 14th October 2022

DOI: 10.1039/d2dt02950b

rsc.li/dalton

Chromium(III) complexes can show phosphorescence from the spin-flip excited doublet states $^2E/^2T_1$ in the near-infrared with high photoluminescence quantum yields and extremely long lifetimes in the absence of dioxygen. The prototype molecular ruby, **[Cr(ddpd)$_2$]$^{3+}$** (ddpd = *N*,*N*′-dimethyl-*N*,*N*′-dipyridine-2-ylpyridine-2,6-diamine), has a photoluminescence quantum yield and a luminescence lifetime of 13.7% and 1.1 ms in deaerated acetonitrile, respectively. However, its luminescence is strongly quenched by $^3O_2$ *via* an efficient Dexter-type energy transfer process. To enable luminescence applications of molecular rubies in solution under aerobic conditions, we explored the potential of sterically demanding ddpd ligands to shield the chromium(III) center from O_2 using steady state and time-resolved photoluminescence spectroscopy. The structures of the novel complexes with sterically demanding ligands were investigated by single crystal X-ray diffraction and quantum chemically by density functional theory calculations. The O_2 sensitivity of the photoluminescence was derived from absolutely measured photoluminescence quantum yields and excited state lifetimes under inert and aerobic conditions and by Stern–Volmer analyses of these data. Optimal sterically shielded chromium(III) complexes revealed photoluminescence quantum yields of up to 5.1% and excited state lifetimes of 518 μs in air-saturated acetonitrile, underlining the large potential of this ligand design approach to broaden the applicability of highly emissive chromium(III) complexes.

Introduction

Research on luminescent first-row transition metal complexes has tremendously increased in recent years to replace and complement the dominating precious and rare earth elements in molecular inorganic photochemistry.[1] Prominent examples are chromium(III) complexes with tridentate ligands and large bite angles which display a strong phosphorescence from spin-flip excited doublet states $^2E/^2T_1$ in the near-infrared (NIR) spectral region with extremely high quantum yields and lifetimes, yet typically only in the absence of molecular oxygen ($^3O_2$).[2–4]

The prototypical complex is the so-called molecular ruby, **[Cr(ddpd)$_2$]$^{3+}$** (**[Cr^{5H}]$^{3+}$**, ddpd = *N*,*N*′-dimethyl-*N*,*N*′-dipyridine-2-ylpyridine-2,6-diamine, Scheme 1a) with a luminescence quantum yield of ϕ_{PL}^{Ar} = 13.7% and an excited state lifetime of τ_{PL}^{Ar} = 1.1 ms at room temperature in deaerated acetonitrile solution (λ_{em} = 738, 775 nm).[5,6] Modifying the ligand structure and substitution pattern enabled the tuning of the emission wavelength from 709 nm to 1067 nm.[7,8]

Several unimolecular non-radiative decay pathways compete with the spin- and Laporte-forbidden radiative relaxation in octahedral chromium(III) complexes. This includes back-intersystem crossing to dissociative quartet states ($^4T_2$; Scheme 1b), excited state distortion,[9] and multiphonon relaxation[10] promoted by CH, NH or OH overtones from ligands or solvent molecules.[3] Large ligand field splitting and rigid ligand frameworks promoting high octahedricity and ligand deuteration helped to increase the quantum yield and lifetime of the excited state of **[Cr^{5H}]$^{3+}$** up to ϕ_{PL}^{Ar} = 30% and τ_{PL}^{Ar} = 2300 μs in O_2-free deuterated acetonitrile solution at room temperature.[12]

The dual NIR emission of **[Cr^{5H}]$^{3+}$** was already exploited for O_2 and ratiometric temperature sensing as well as to optically probe hydrostatic pressure.[13] The effective quenching of the chromium(III) emission by $^3O_2$ leads to a high quantum yield of the formed singlet oxygen ($\Phi(^1O_2)$ *ca.* 61% in acetonitrile),[14] enabling the usage of **[Cr^{5H}]$^{3+}$** as $^1O_2$-generating photosensitizer for organic photo-oxidation reactions[14] and photodynamic therapy.[15] However, the high sensitivity to $^3O_2$ limits other potentially interesting applications of chromium(III) complexes

[a]*Department of Chemistry, Johannes Gutenberg University of Mainz, Mainz, Germany. E-mail: katja.heinze@uni-mainz.de*
[b]*Division Biophotonics, Federal Institute for Materials Research and Testing (BAM), Richard-Willstätter-Straße 11, 12489 Berlin, Germany*

†Electronic supplementary information (ESI) available. CCDC 2125019–2125021. For ESI and crystallographic data in CIF or other electronic format see DOI: https://doi.org/10.1039/d2dt02950b

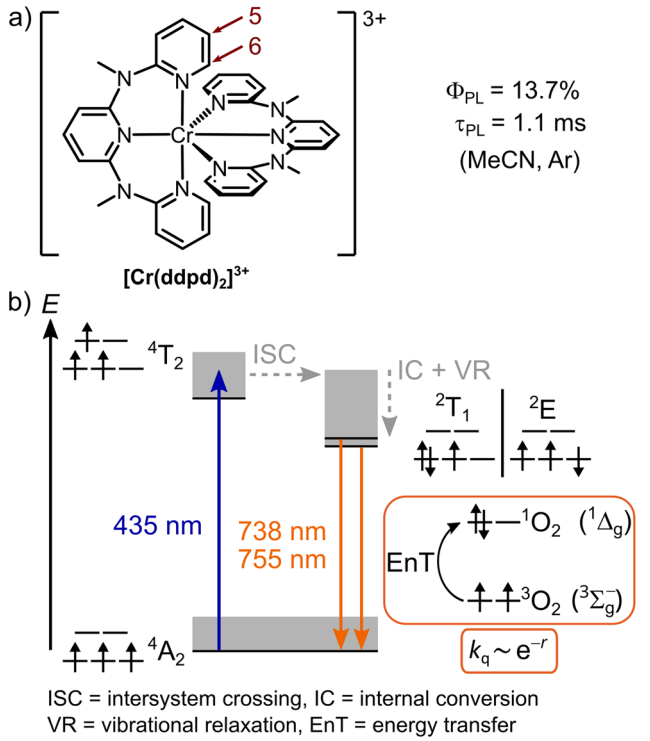

Scheme 1 a) Molecular structure of $[Cr^{5H}]^{3+}$ including the atom numbering of the ligand and (b) schematic Jablonski diagram of a transition metal complex with d^3 electron configuration in an octahedral environment with a large ligand field splitting. Relevant microstates and term symbols are indicated. The optical-spectroscopic data are given for $[Cr^{5H}]^{3+}$ in acetonitrile solution at room temperature. Dexter-type energy transfer from doublet excited states to triplet oxygen ($^3\Sigma_g^-$) is indicated by respective microstates and term symbols.[5,11] The grey boxes indicate vibrational levels.

as optical reporters, in bioimaging, and energy conversion schemes.

Mechanistically, quenching of long-lived electronically excited states with multiplicities differing from the ground state multiplicity by $^3O_2$ follows the Dexter energy transfer mechanism.[11] The doublet excited states of chromium(III) complexes are well suited to sensitize $^1O_2$ generation due to their much higher energy than the $^1O_2$ energy (ΔE = 0.6 eV), the favorable spin-statistics (67%), and the up to millisecond lifetimes of the excited doublet states.[5] Based on the overlap of the donor and acceptor wavefunctions, the Dexter energy transfer rate constant k_q decreases exponentially with the donor–acceptor distance,[16] which is typically below 10 Å.[17] To prevent this deactivation pathway, photoreactions, spectroscopic measurements and applications employing photoactive transition metal complexes are usually carried out under O_2-free conditions.[4,18] One strategy to protect the O_2-sensitive luminophores from oxygen is to embed them in O_2-impermeable matrices.[18] For example, encapsulation of the molecular ruby in polystyrene nanoparticles coated with a silica shell and embedded in an oxygen-barrier poly(vinyl alcohol) film increased the quantum yield under air from ϕ_{PL}^{air} < 1% to ϕ_{PL}^{air} = 15.2%.[6]

In the present study, we follow a different approach exploiting a rational ligand design concept: the coordinating ddpd ligand is derivatized with substituents of increasing bulkiness to mitigate close contacts of the chromium(III) center and O_2 and hence to reduce the overlap of their wavefunctions. The increased average Cr···O_2 distance is expected to decrease the Dexter energy transfer rate constant k_q, thereby reducing the O_2-sensitivity of the chromium(III) complexes and increasing the photoluminescence quantum yields ϕ_{PL}^{air} and lifetimes τ_{PL}^{air} in air-saturated systems.

Results and discussion

DFT calculations

The position at the ddpd ligand closest to the chromium(III) center with arguably the strongest shielding effect is the 6-position (Scheme 1a). According to density functional theory (DFT) modeling, the 6-methyl substituted derivative $ddpd^{6Me}$ coordinates to chromium(III) giving $[Cr(ddpd^{6Me})_2]^{3+}$ ($[Cr^{6Me}]^{3+}$, Fig. 1b), however with significantly increased Cr–N distances to the terminal pyridines by 0.1 Å compared to the parent complex $[Cr^{5H}]^{3+}$ (Table S3†). Possibly, interligand steric congestion, as observed in iron(II) complexes with 6,6″-halogenated 2,2′:6′,2″-terpyridyl (tpy) ligands,[20] hinders the successful coordination of $ddpd^{6Me}$ to the small chromium(III) ion (ionic radius 0.62 Å).[21] Therefore, all attempts to coordinate $ddpd^{6Me}$ to chromium(III) to form $[Cr^{6Me}]^{3+}$ failed. The next suitable position for introducing a shielding substituent R is position 5 at the terminal pyridine rings to give the $ddpd^{5R}$ ligands (Scheme 1a). As these substituents R point away from the metal center, the substituent size clearly plays a key role to efficiently block the access of O_2 to the chromium center (Fig. 1). Therefore, we prepared ddpd ligands with methyl, mesityl and 2,4,6-triisopropylphenyl substituents at position 5 ($ddpd^{5Me}$, $ddpd^{5Mes}$ and $ddpd^{5Tripp}$) and the corresponding chromium(III) complexes $[Cr(ddpd^{5Me})_2][BF_4]_3$ ($[Cr^{5Me}][BF_4]_3$), $[Cr(ddpd^{5Mes})_2][BF_4]_3$ ($[Cr^{5Mes}][BF_4]_3$) and $[Cr(ddpd^{5Tripp})_2][BF_4]_3$ ($[Cr^{5Tripp}][BF_4]_3$). Space-filling models of the DFT optimized complex geometries demonstrate the increasing steric demand of the ligand around the metal center (Fig. 1c–e).

Synthesis and characterization

The $ddpd^{5R}$ ligands were synthesized according to the procedures outlined in Scheme 2 and analytically characterized (see ESI†).[22] The methyl derivative $ddpd^{5Me}$ was prepared from 2,6-diaminopyridine and 2-bromo-5-methyl pyridine followed by *N*-methylation with methyl iodide (Scheme 2a). The required 2-(*N*-methyl)-amino-5-aryl pyridines py^{5Mes}-NHMe and py^{5Tripp}-NHMe were obtained from 2,5-dibromopyridine by amination of the 2-position followed by Suzuki coupling of the 5-position with the respective aryl boronic acid (Scheme 2b). *N*-Substitution of py^{5Mes}-NHMe and py^{5Tripp}-NHMe with 2,6-dibromopyridine yielded the tridentate ligands $ddpd^{5Mes}$ and $ddpd^{5Tripp}$, respectively (Scheme 2b).

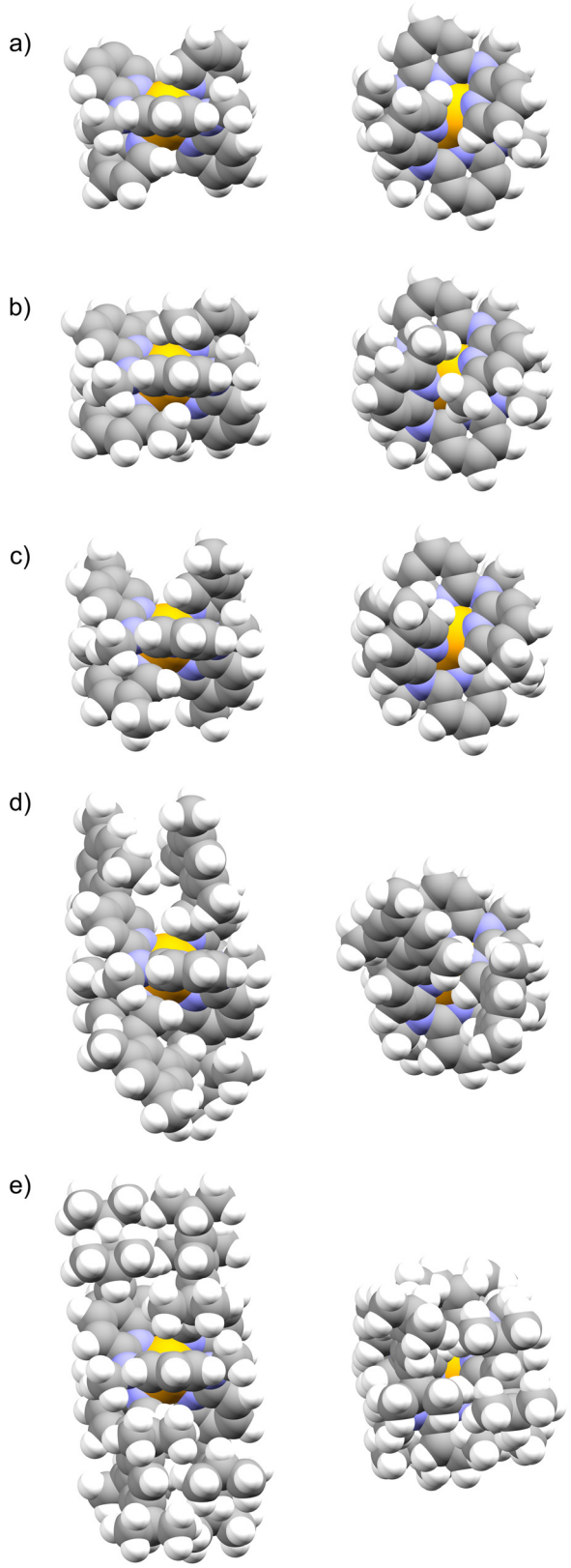

Fig. 1 Space-filling models of (a) $[Cr(ddpd)_2]^{3+}$, (b) $[Cr(ddpd^{6Me})_2]^{3+}$, (c) $[Cr(ddpd^{5Me})_2]^{3+}$, (d) $[Cr(ddpd^{5Mes})_2]^{3+}$ and (e) $[Cr(ddpd^{5Tripp})_2]^{3+}$ from DFT calulcations demonstrating the increasing shielding of the chromium center (orange: Cr, blue: N, grey: C, white: H). Left: front view, right: top view.

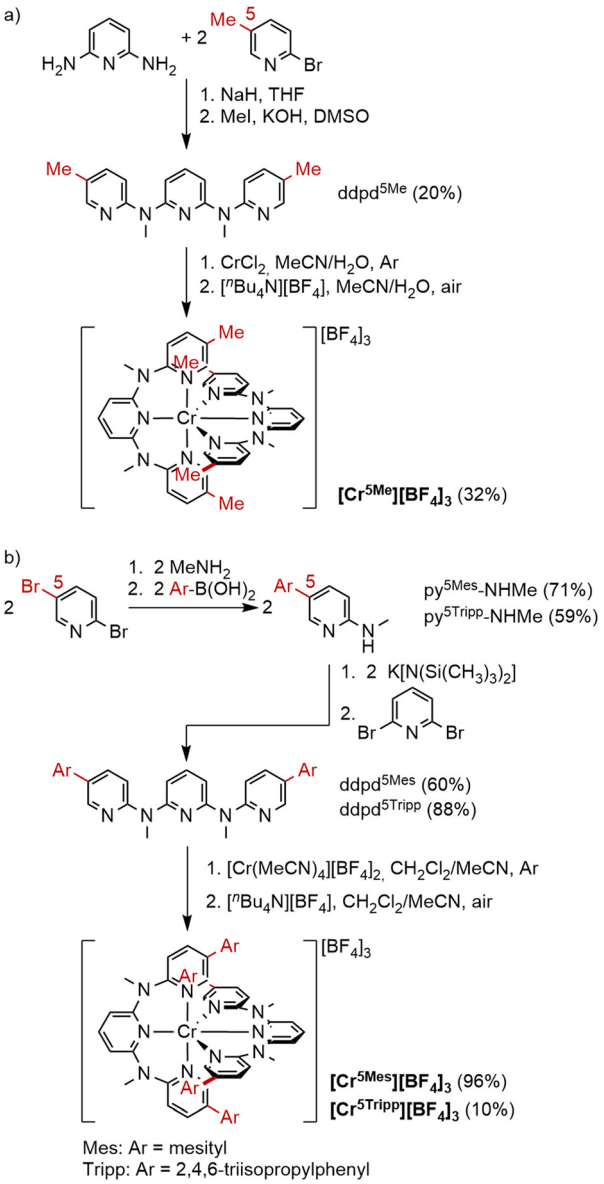

Scheme 2 Syntheses of substituted ligands $ddpd^{5R}$ and corresponding chromium(III) complexes $[Cr(ddpd^{5R})_2][BF_4]_3$.

Coordination of $ddpd^{5Me}$ to chromium(III) was successful using a procedure analogous to the preparation of $[Cr^{5H}][BF_4]_3$ in $MeCN/H_2O$ giving $[Cr^{5Me}][BF_4]_3$ (Scheme 2a).[5] The aryl substituted ligands $ddpd^{5Mes}$ and $ddpd^{5Tripp}$, however, are only poorly soluble in $MeCN/H_2O$ mixtures. Consequently, different solvents and a different chromium precursor were required. With $[Cr(MeCN)_4][BF_4]_2$[23] in $MeCN/CH_2Cl_2$, these bulky ligands were successfully coordinated to chromium(II), yielding $[Cr^{5Mes}][BF_4]_3$ and $[Cr^{5Tripp}][BF_4]_3$, respectively, after oxidation (Scheme 2b). Slow diffusion of diethyl ether into concentrated acetonitrile solutions of $[Cr^{5Me}][BF_4]_3$, $[Cr^{5Mes}][BF_4]_3$ and $[Cr^{5Tripp}][BF_4]_3$ yielded orange crystals suitable for X-ray diffraction analyses (Table 2). As derived from DFT optimized geometries and crystal structures (Tables 1, 2 and S1–S3†), in these

Table 1 Selected bond lengths/Å and angles/° of complexes $[Cr^{5R}]^{3+}$ obtained from DFT calculations

	$[Cr^{5H}]^{3+}$	$[Cr^{5Me}]^{3+}$	$[Cr^{5Mes}]^{3+}$	$[Cr^{5Tripp}]^{3+}$
Cr–N1	2.059	2.056	2.062	2.064
Cr–N2	2.046	2.048	2.038	2.041
Cr–N3	2.059	2.056	2.057	2.060
Cr–N4	2.059	2.055	2.068	2.062
Cr–N5	2.046	2.047	2.045	2.044
Cr–N6	2.059	2.055	2.059	2.060
N1–Cr–N2	86.46	86.49	85.65	84.95
N2–Cr–N3	86.46	86.42	86.97	85.11
N1–Cr–N3	172.92	172.91	172.49	170.06
N4–Cr–N5	86.46	86.46	86.06	85.07
N5–Cr–N6	86.46	86.49	87.58	85.13
N4–Cr–N6	172.92	172.95	173.13	170.20
S(OC-6)[19]	0.26	0.26	0.32	0.52

complexes, a slight deviation from octahedral symmetry results with the largest substituent Tripp with the shape parameter[19] S(OC-6) > 0.5. In the solid state, the average Cr–N bond from the central pyridines to the metal center is shortened (2.042 Å to 2.023 Å), while the average Cr–N bond to the terminal pyridines is elongated from 2.045 Å to 2.053 Å. Simultaneously, the intramolecular N–Cr–N angles increasingly deviate from 90° and 180° within this series. This is expected as the size of the aromatic substituents forces the ligand scaffold to twist more strongly out of plane than with small substituents like R = H or Me. Due to the torsion induced by the bulky Tripp substituent, the dihedral angle between the central pyridine planes becomes smaller ($\measuredangle$10°, Table S1†) compared to the other ligands ($\measuredangle$14°–19°). The more efficient overlap of the pyridine and metal centered t_{2g} orbitals presumably causes a stronger nephelauxetic effect and a bathochromic shift of the emission band for this complex (see below). Moreover, intermolecular π–π stacking occurs between the aromatic substituents (centroid-to-centroid distance in $[Cr^{5Mes}][BF_4]_3$ = 4.961 Å, Fig. S21† and $[Cr^{5Tripp}][BF_4]_3$ 5.700 Å, Fig. S22†) and even intramolecular interligand π–π stacking was observed in $[Cr^{5Tripp}][BF_4]_3$ (5.968 Å). This intramolecular π–π stacking might shield the chromium ion even more efficiently from the environment (Fig. 1e).

As a measure of the accessibility of the metal center within the ligand scaffold for subsequent luminescence studies without and in the presence of oxygen, the shortest Cr···F (BF_4^-) and Cr···N (MeCN) distances in the crystal structures were taken into account (Table S1 and Fig. S20–22†). Compared to the complex with R = Me, the distances to the counter ions increase, while they remain in the same range for MeCN contacts. This suggests better shielding from tetrahedral molecules than from linear molecules as well as a weaker electrostatic interaction between the counter ions and the cationic metal center in the solid state.

Optical properties of $[Cr(ddpd^{5R})_2][BF_4]_3$

The absorption and photoluminescence spectra of $[Cr^{5R}][BF_4]_3$ complexes with R = H, Me, Mes, Tripp were recorded in acetonitrile at room temperature under anaerobic conditions (Fig. 2a). The shapes of the respective absorption and emission spectra are relatively similar. Bathochromic shifts are noted for the $^4A_2 \rightarrow {}^4T_2$/LMCT absorption band from 435 to 455 nm (Fig. S23a†) and for the spin-flip emission bands from 738 nm → 742 nm/775 nm → 794 nm (Table 3 and Fig. 2). The bathochromic shift of the $^4A_2 \rightarrow {}^4T_2$ absorption band, combined with the more intense ligand-to-metal charge transfer absorption band, could be reproduced by time-dependent DFT calculations (Fig. S24†). The π–π* transitions of the ligands in the UV region display larger changes, in particular for complexes with aryl substituted ligands (Fig. 2a), which is already evident from the ligand absorption bands (Fig. S13†). The quantum yields ϕ_{PL}^{Ar} and luminescence lifetimes τ_{PL}^{Ar} of the complexes in Ar-saturated acetonitrile solution are very similar (Table 4).

Oxygen quenching experiments

The photoluminescence of the complexes $[Cr^{5R}][BF_4]_3$ is quenched in the presence of O_2, yet to very different extents (Table 4, Fig. 2 and S25†). The luminescence properties of $[Cr^{5H}][BF_4]_3$ and $[Cr^{5Me}][BF_4]_3$ in air-saturated acetonitrile solution are very similar, demonstrating that the shielding by methyl groups in position 5 is not effective. The DFT modeling and XRD data of the complexes with R = H and Me confirm

Table 2 Selected bond lengths/Å and angles/° of complexes $[Cr^{5R}][BF_4]_3$ obtained from single crystal XRD analyses

	$[Cr^{5H}][BF_4]_3$ [5]	$[Cr^{5Me}][BF_4]_3$	$[Cr^{5Mes}][BF_4]_3$	$[Cr^{5Tripp}][BF_4]_3$
Cr–N1	2.0485(18)	2.0448(14)	2.0577(17)	2.0523(14)
Cr–N2	2.0393(18)	2.0294(14)	2.0268(17)	2.0222(14)
Cr–N3	2.0394(19)	2.0471(14)	2.0623(18)	2.0561(14)
Cr–N4	2.0446(17)	2.0492(13)	2.0579(18)	2.0576(14)
Cr–N5	2.0444(18)	2.0300(14)	2.0215(17)	2.0238(14)
Cr–N6	2.0485(18)	2.0403(13)	2.0549(18)	2.0449(14)
N1–Cr–N2	85.13(8)	85.83(6)	87.63(7)	84.91(6)
N2–Cr–N3	85.74(7)	86.18(6)	86.23(7)	85.26(6)
N1–Cr–N3	170.86(8)	172.00(5)	173.44(7)	170.02(6)
N4–Cr–N5	85.89(7)	86.00(5)	85.91(7)	84.48(5)
N5–Cr–N6	84.99(7)	86.08(5)	86.74(7)	84.98(6)
N4–Cr–N6	170.88(7)	171.81(5)	172.62(7)	169.35(6)
Cr···F (BF_4^-)	5.438(4)	4.682(2)	6.768(2)	5.556(2)
Cr···N (MeCN)	4.613(4)	4.694(2)	4.654(2)	4.513(2)
S(OC-6)[19]	0.43	0.35	0.31	0.56

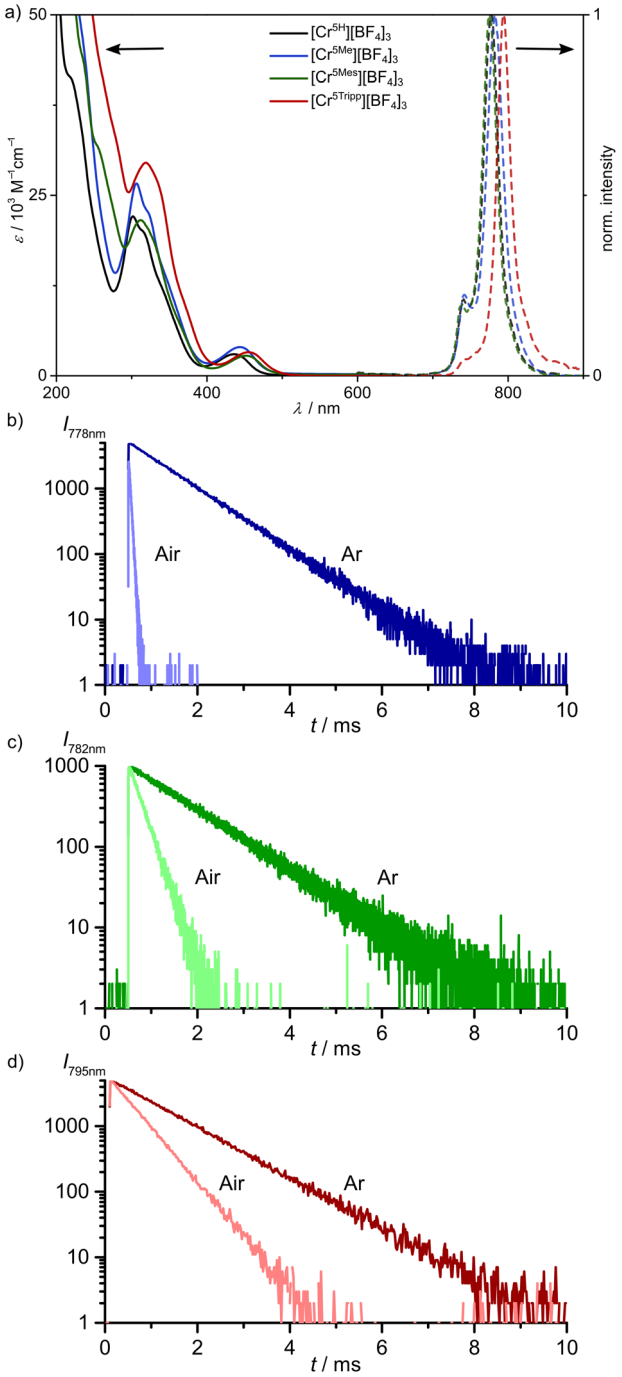

Fig. 2 (a) Absorption and normalized emission spectra of $[Cr^{5R}][BF_4]_3$ complexes with R = H (λ_{exc} = 435 nm, black), Me (λ_{exc} = 441 nm, blue), Mes (λ_{exc} = 450 nm, green) and Tripp (λ_{exc} = 454 nm, red) in Ar-saturated acetonitrile. Luminescence decays of $[Cr^{5R}][BF_4]_3$ complexes with (b) R = Me, (c) R = Mes, (d) R = Tripp in air- and Ar-saturated acetonitrile solution at 293 K.

this assumption as the accessibility of the chromium(III) ion seems to be very similar for both complexes (Fig. 1). On the other hand, mesityl and 2,4,6-triisopropyl substituents in position 5 clearly affect the photoluminescence quantum yields and luminescence lifetimes of the chromium(III) complexes in

Table 3 Optical data of the $[Cr^{5R}][BF_4]_3$ complexes in Ar-saturated acetonitrile solution at 293 K

Complex	λ_{max}/nm (ε/10^3 M^{-1} cm^{-1})	λ_{em}/nm (λ_{exc}/nm)
$[Cr^{5Me}][BF_4]_3$	444 (4), 323 (23, sh), 305 (27), 225 (53, sh)	741, 779 (441)
$[Cr^{5Mes}][BF_4]_3$	453 (3), 312 (22), 257 (31), 236 (44, sh)	742, 782 (453)
$[Cr^{5Tripp}][BF_4]_3$	455 (3), 319 (30), 240 (55, sh)	740 (sh), 794 (455)

air-saturated acetonitrile as reflected by ϕ_{PL}^{air} = 2.2% and 5.1% and τ_{PL}^{air} = 244 μs and 518 μs, respectively. Compared to R = H and Me, where the ratios of $\phi_{PL}^{Ar}/\phi_{PL}^{air}$ and $\tau_{PL}^{Ar}/\tau_{PL}^{air}$ amount to 17–25, for the Tripp substituted complex, these ratios drop remarkably to two (Table 4). This demonstrates the efficient shielding of the chromium(III) center from O_2 by the bulky Tripp substituents.

Compared to very recently reported chromium(III) complexes with 1,3-bis(2′-pyridylimino)-isoindoline ligands reported as showing long-lived NIR emission under inert and ambient conditions in acetonitrile (τ_{PL}^{Ar} = 8.0 μs and 25.0 μs; τ_{PL}^{air} = 4.5 μs and 8.1 μs),[24] the here reported lifetimes of $[Cr^{5Mes}][BF_4]_3$ and $[Cr^{5Tripp}][BF_4]_3$ are larger by factors of 30 to 115.

Emission intensity and lifetime-based Stern–Volmer analyses with varying concentrations or partial pressures of O_2 in acetonitrile solution gave linear plots with Stern–Volmer constants K_{SV}^{Int} and K_{SV}^{LT} matching within the measurement uncertainty. This confirms the diffusional quenching by O_2 (Table 4, Fig. 3 and S25†). The K_{SV}^{Int} and K_{SV}^{LT} values drop significantly from $K_{SV} \approx 0.13$ hPa^{-1} for $[Cr^{5H}][BF_4]_3$ and $[Cr^{5Me}][BF_4]_3$ over 0.02 hPa^{-1} for $[Cr^{5Mes}][BF_4]_3$ to 0.01 hPa^{-1} for $[Cr^{5Tripp}][BF_4]_3$. Similarly, the quenching rate constants $k_q = K_{SV}/\tau_{PL}^{Ar}$ decrease from ≈ 110 hPa s^{-1} for $[Cr^{5H}][BF_4]_3$ and $[Cr^{5Me}][BF_4]_3$ over 20 hPa s^{-1} for $[Cr^{5Mes}][BF_4]_3$ to 11 hPa s^{-1} for $[Cr^{5Tripp}][BF_4]_3$, equaling an overall shielding-related reduction by a factor of about 10. These results clearly demonstrate the superior shielding effect of the bulky ddpd^{5Tripp} ligand.

Cooling the complexes under aerobic and anaerobic conditions increases the luminescence lifetimes (Fig. S26 and Table S4†) of the complexes $[Cr^{5R}][BF_4]_3$ in acetonitrile solution, yet displaying a different degree of the temperature dependence for deaerated and atmospheric conditions (Fig. S27†). Under Ar-saturated conditions, for R = H, Me, Mes, the lifetimes are prolonged by a factor of f = 5–7 upon cooling from 338 to 278 K. For the bulky substituent R = Tripp, the temperature dependence is significantly smaller (factor of f = 2.4) under these conditions. This indicates a higher activation barrier for thermally induced non-radiative processes, probably because the substituent Tripp enforces a rigid structure of the respective chromium(III) complex. Under atmospheric conditions, the increase in the luminescence lifetimes upon lowering the temperature is less significant for all complexes (R = H: $f \approx 1.1$, Me: $f \approx 1.3$; Mes: $f \approx 2.5$, Tripp: $f \approx 1.8$). Especially for the complexes with the ddpd ligands bearing the small substituents R = H and Me, O_2 quenching is now the most sig-

Table 4 Luminescence and O_2-quenching Stern–Volmer data of the $[Cr^{5R}][BF_4]_3$ complexes in acetonitrile solution at 293 K

	$[Cr^{5H}][BF_4]_3$ [5,6]	$[Cr^{5Me}][BF_4]_3$	$[Cr^{5Mes}][BF_4]_3$	$[Cr^{5Tripp}][BF_4]_3$
λ_{obs}/nm	778	778	782	795
ϕ_{PL}^{Ar}/%	13.7	13.9	12.1	11.3
τ_{PL}^{Ar}/μs	1122	1258	1173	1131
ϕ_{PL}^{air}/%	0.8	0.8	2.2	5.1
τ_{PL}^{air}/μs	52	52	244	518
$\phi_{PL}^{Ar}/\phi_{PL}^{air}$	17	17	5	2
$\tau_{PL}^{Ar}/\tau_{PL}^{air}$	20	25	5	2
K_{SV}^{Int}/hPa^{-1}	0.116	0.135	0.023	0.012
K_{SV}^{LT}/hPa^{-1}	0.123	0.147	0.024	0.012
k_q^{int}/hPa s^{-1}	103.3	107.4	19.4	10.7
k_q^{LT}/hPa s^{-1}	109.6	116.5	20.0	10.5

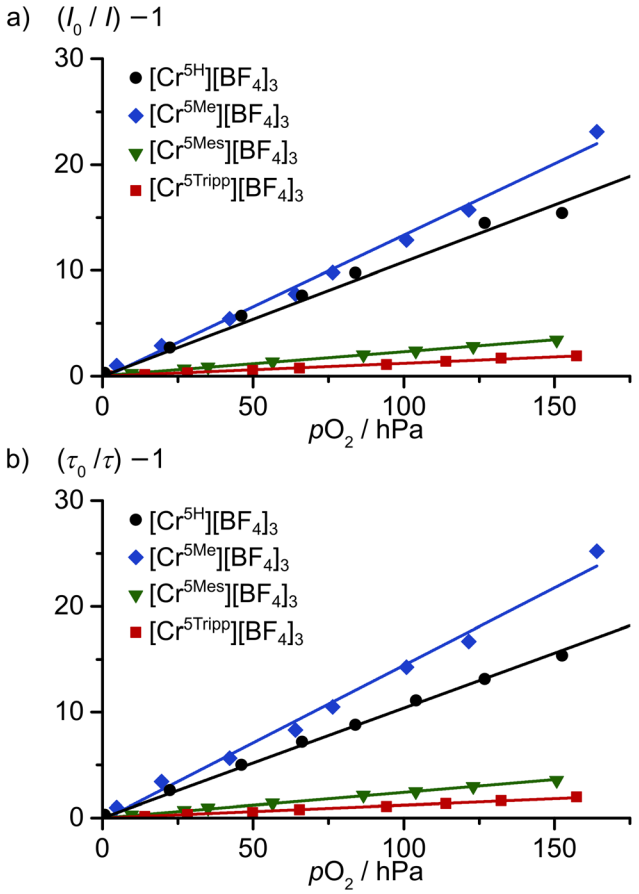

Fig. 3 (a) Intensity- and (b) lifetime-based Stern–Volmer plots of the $[Cr^{5R}][BF_4]_3$ complexes with O_2 in acetonitrile at 293 K.

nificant non-radiative decay process, as it is faster than other unimolecular, non-radiative (temperature-dependent) pathways.

Conclusion

This study reports the syntheses and structures of novel chromium(III) spin-flip emitters (molecular rubies) modified at position 5 of the tridentate chelate ligands with bulky substituents to protect the chromium(III) center from O_2 quenching. Conceptually, the shielding of a spin-flip emitter from quenching by $^3O_2$ is more straightforward than the shielding of a phosphorescent charge-transfer emitter due to the metal-localized and ligand-delocalized nature of the respective participating wavefunctions. While small methyl substituents barely show a protective effect, the aryl substituents mesityl and 2,4,6-triisopropylphenyl effectively shield the chromium(III) center from a close contact with O_2. This reduces the Dexter-type energy transfer rate to O_2 from $k_q \approx 110$ hPa s^{-1} to 11 hPa s^{-1} and consequently increases the photoluminescence quantum yields and lifetimes of the respective chromium(III) complexes from 0.8 to 5.1% and from 52 to 518 μs, respectively, in air-saturated acetonitrile solution at 293 K. In the future, these favorable luminescence features of the chromium(III) complexes with sterically demanding ddpd ligands can enable applications of shielded molecular rubies, for example as reporters in time-gated luminescence detection schemes[25] or for circularly polarized NIR emission[26] under aerobic conditions.

Author contributions

L. S. performed the synthesis, characterization, DFT, UV-VIS, the quantum yield and lifetime measurements under Ar and air and temperature-dependent emission measurements under Ar and air, visualized the data and wrote the original draft. C. W. performed the oxygen-dependent Stern–Volmer studies and preliminary optical characterization. C. F. solved and refined the crystal structures. U. R.-G. supervised the Stern–Volmer studies and revised the manuscript. K. H. designed and supervised the project and finalized the manuscript.

Conflicts of interest

There are no conflicts to declare.

Acknowledgements

The authors acknowledge Dr Luca M. Carrella and Dr Dieter Schollmeyer for collection of XRD data and Dr Robert

Naumann for support with the experimental setup for QY measurements. This work was supported by the Deutsche Forschungsgemeinschaft (RE 1203/23-1 and RE1203/23-2, HE 2778/10-2) and through grant INST 247/1018-1 FUGG to KH. Parts of this research were conducted using the supercomputer Elwetritsch and advisory services offered by the TU Kaiserslautern (**https://elwe.rhrk.uni-kl.de**) which is a member of the AHRP.

References

1 (*a*) C. Wegeberg and O. S. Wenger, *JACS Au*, 2021, **1**, 1860–1876; (*b*) C. Förster and K. Heinze, *Chem. Soc. Rev.*, 2020, **49**, 1057–1070.
2 (*a*) P. A. Scattergood, in *Organometallic Chemistry*, ed. N. J. Patmore and P. I. P. Elliott, Royal Society of Chemistry, Cambridge, 2020, vol. 43, pp. 1–34; (*b*) J.-R. Jiménez, B. Doistau, M. Poncet and C. Piguet, *Coord. Chem. Rev.*, 2021, **434**, 213750.
3 S. Otto, M. Dorn, C. Förster, M. Bauer, M. Seitz and K. Heinze, *Coord. Chem. Rev.*, 2018, **359**, 102–111.
4 W. R. Kitzmann, J. Moll and K. Heinze, *Photochem. Photobiol. Sci.*, 2022, **21**, 1309–1331.
5 S. Otto, M. Grabolle, C. Förster, C. Kreitner, U. Resch-Genger and K. Heinze, *Angew. Chem., Int. Ed.*, 2015, **54**, 11572–11576.
6 C. Wang, W. R. Kitzmann, F. Weigert, C. Förster, X. Wang, K. Heinze and U. Resch-Genger, *ChemPhotoChem*, 2022, e202100296.
7 F. Reichenauer, C. Wang, C. Förster, P. Boden, N. Ugur, R. Báez-Cruz, J. Kalmbach, L. M. Carrella, E. Rentschler, C. Ramanan, G. Niedner-Schatteburg, M. Gerhards, M. Seitz, U. Resch-Genger and K. Heinze, *J. Am. Chem. Soc.*, 2021, **143**, 11843–11855.
8 N. Sinha, J.-R. Jiménez, B. Pfund, A. Prescimone, C. Piguet and O. S. Wenger, *Angew. Chem., Int. Ed.*, 2021, **60**, 23722–23728.
9 (*a*) M. W. Perkovic, M. J. Heeg and J. F. Endicott, *Inorg. Chem.*, 1991, **30**, 3140–3147; (*b*) A. M. McDaniel, H.-W. Tseng, N. H. Damrauer and M. P. Shores, *Inorg. Chem.*, 2010, **49**, 7981–7991.
10 E. Kreidt, C. Kruck and M. Seitz, in *Handbook on the physics and chemistry of rare earths. Including actinides*, ed. J.-C. G. Bünzli, V. K. Pecharsky, G.-Y. Adachi, K. A. Gschneider and E. LeRoy, North-Holland, Amsterdam, Oxford, 2018, vol. 53, pp. 35–79.
11 D. L. Dexter, *J. Chem. Phys.*, 1953, **21**, 836–850.
12 C. Wang, S. Otto, M. Dorn, E. Kreidt, J. Lebon, L. Sršan, P. Di Martino-Fumo, M. Gerhards, U. Resch-Genger, M. Seitz and K. Heinze, *Angew. Chem., Int. Ed.*, 2018, **57**, 1112–1116.
13 (*a*) S. Otto, N. Scholz, T. Behnke, U. Resch-Genger and K. Heinze, *Chem. – Eur. J.*, 2017, **23**, 12131–12135; (*b*) S. Otto, J. P. Harris, K. Heinze and C. Reber, *Angew. Chem., Int. Ed.*, 2018, **57**, 11069–11073; (*c*) C. Wang, S. Otto, M. Dorn, K. Heinze and U. Resch-Genger, *Anal. Chem.*, 2019, **91**, 2337–2344.
14 S. Otto, A. M. Nauth, E. Ermilov, N. Scholz, A. Friedrich, U. Resch-Genger, S. Lochbrunner, T. Opatz and K. Heinze, *ChemPhotoChem*, 2017, **1**, 344–349.
15 U. Basu, S. Otto, K. Heinze and G. Gasser, *Eur. J. Inorg. Chem.*, 2019, 37–41.
16 F. Strieth-Kalthoff, M. J. James, M. Teders, L. Pitzer and F. Glorius, *Chem. Soc. Rev.*, 2018, **47**, 7190–7202.
17 V. Balzani, G. Bergamini, S. Campagna and F. Puntoriero, in *Photochemistry and Photophysics of Coordination Compounds I*, ed. V. Balzani and S. Campagna, Springer Berlin Heidelberg, Berlin, Heidelberg, 2007, vol. 280, pp. 1–36.
18 D. M. Arias-Rotondo and J. K. McCusker, *Chem. Soc. Rev.*, 2016, **45**, 5803–5820.
19 P. Alemany, D. Casanova, S. Alvarez, C. Dryzun and D. Avnir, in *Reviews in Computational Chemistry*, ed. A. L. Parrill and K. B. Lipkowitz, Wiley, Hoboken, NJ, 2017, pp. 289–352.
20 S. M. Fatur, S. G. Shepard, R. F. Higgins, M. P. Shores and N. H. Damrauer, *J. Am. Chem. Soc.*, 2017, **139**, 4493–4505.
21 U. Müller, *Anorganische Strukturchemie*, Vieweg+Teubner, Wiesbaden, 6th edn, 2008.
22 (*a*) C. Förster, M. Dorn, T. Reuter, S. Otto, G. Davarci, T. Reich, L. Carrella, E. Rentschler and K. Heinze, *Inorganics*, 2018, **6**, 86; (*b*) J. Tasseroul, M. M. Lorenzo-Garcia, J. Dosso, F. Simon, S. Velari, A. de Vita, P. Tecilla and D. Bonifazi, *J. Org. Chem.*, 2020, **85**, 3454–3464; (*c*) A. Breivogel, C. Förster and K. Heinze, *Inorg. Chem.*, 2010, **49**, 7052–7056.
23 R. A. Heintz, J. A. Smith, P. S. Szalay, A. Weisgerber and K. R. Dunbar, in *Inorganic syntheses*, ed. D. Coucouvanis, Wiley-Interscience, New York, 2002, vol. 33, pp. 75–121.
24 N. Sawicka, C. J. Craze, P. N. Horton, S. J. Coles, E. Richards and S. J. A. Pope, *Chem. Commun.*, 2022, **58**, 5733–5736.
25 W. Yang and S.-L. Chen, *J. Innovative Opt. Health Sci.*, 2020, **13**, 2030006.
26 (*a*) J.-R. Jiménez, B. Doistau, C. M. Cruz, C. Besnard, J. M. Cuerva, A. G. Campaña and C. Piguet, *J. Am. Chem. Soc.*, 2019, **141**, 13244–13252; (*b*) C. Dee, F. Zinna, W. R. Kitzmann, G. Pescitelli, K. Heinze, L. Di Bari and M. Seitz, *Chem. Commun.*, 2019, **55**, 13078–13081; (*c*) J.-R. Jiménez, M. Poncet, S. Míguez-Lago, S. Grass, J. Lacour, C. Besnard, J. M. Cuerva, A. G. Campaña and C. Piguet, *Angew. Chem., Int. Ed.*, 2021, **60**, 10095–10102.